HHS Public Access

Author manuscript

Appl Mater Today. Author manuscript; available in PMC 2021 December 01.

Published in final edited form as:

Appl Mater Today. 2020 December ; 21: . doi:10.1016/j.apmt.2020.100860.

Nanoclay Promotes Mouse Cranial Bone Regeneration Mainly through Modulating Drug Binding and Sustained Release

Jue Hu[a,b], **Jacob M. Miszuk**[a,b], **Kyle M. Stein**[a], **Hongli Sun**[a,b,*]

[a]Department of Oral and Maxillofacial Surgery, University of Iowa College of Dentistry, Iowa City, IA 52242, USA

[b]Iowa Institute for Oral Health Research, University of Iowa College of Dentistry, Iowa City, IA 52242, USA

Abstract

Nanoclay (Nanosilicates, NS) is appearing as an intriguing 2D nanomaterial for bone tissue engineering with multiple proposed functions, e.g., intrinsic osteoinductivity, improving mechanical properties, and drug release capacity. However, the mechanism of NS for *in vivo* bone regeneration has been hardly defined so far. This knowledge gap will significantly affect the design/application of NS-based biomaterials. To determine the role of NS in osteoblastic differentiation and bone formation, we used the mouse calvarial-derived pre-osteoblasts (MC3T3-E1) and a clinically-relevant mouse cranial bone defect model. Instead of a hydrogel, we prepared biomimetic 3D gelatin nanofibrous scaffolds (GF) and NS-blended composite scaffolds (GF/NS) to determine the essential role of NS in critical low-dose (0.5 μg per scaffold) of BMP2-induced cranial bone regeneration. In contrast to "osteoinductivity", our data indicated that NS could enable single-dose of BMP2, promoting significant osteoblastic differentiation while multiple-dose of BMP2 (without NS) was required to achieve similar efficacy. Moreover, our release study revealed that direct binding to NS in GF scaffolds provided stronger protection to BMP2 and sustained release compared to GF/NS composite scaffolds. Consistently, our *in vivo* data indicated that only BMP2/NS direct binding treatment was able to repair the large mouse cranial bone defects after 6 weeks of transplantation while neither BMP2, NS alone, nor BMP2 released from GF/NS scaffolds was sufficient to induce significant cranial bone defect repair. Therefore, we concluded that direct nanoclay-drug binding enabled sustained release is the most critical contribution to the significantly improved bone regeneration compared to other possible mechanisms based on our study.

Graphical Abstract

*Corresponding Authors: Professor Hongli Sun, Ph.D., Department of Oral and Maxillofacial Surgery, Iowa Institute for Oral Health Research, N405 DSB, College of Dentistry, 801 Newton Road, The University of Iowa, Iowa City, IA 52242, Tel: 319-335-1217, hongli-sun@uiowa.edu.

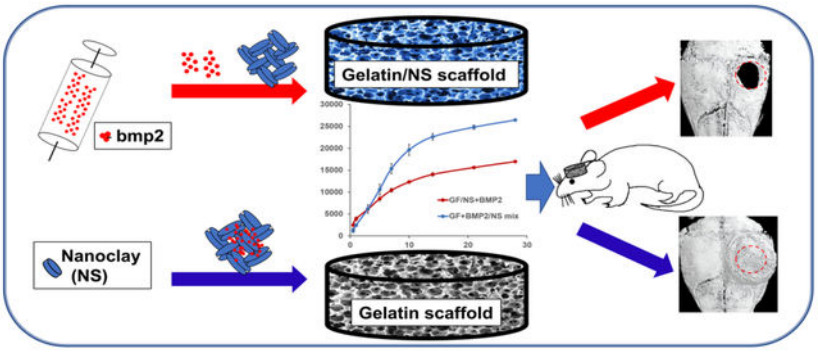

Keywords

Nanoclays; Sustained drug release; Cranial bone regeneration; 3D nanofibrous scaffolds; BMPs; Bone tissue engineering

1. Introduction:

The incidence and repair of large bone defects remains a persistent challenge in clinical surgery today [1, 2]. Autogenous bone grafting is the gold standard avenue for treatment, though it is significantly limited by availability and the risk of donor site morbidity [1, 3, 4]. Biomaterial-mediated growth factor (for example, bone morphogenetic proteins, BMPs) delivery is a promising alternative tissue engineering strategy to combat the limited availability of autologous bone grafts [5]. However, the serious side effects derived from high doses of exogenous drugs, including FDA-approved BMP2 [6–8], have urged us to develop innovative biomaterials and drug delivery techniques to promote strong endogenous bone regeneration [9–14].

Nanoclay (also known as Laponite XLG or Nanosilicates, NS), synthetic smectite ($Na^{+}_{0.7}[(Si_8Mg_{5.5}Li_{0.3})O_{20}(OH)_4]^{-}_{0.7}$), is emerging as an intriguing two-dimensional (2D) nanomaterial for bone tissue engineering, while the potential mechanisms are largely unknown and even controversial based on current reports [15–21]. One unique feature of NS is its potential osteoinductivity, because NS can induce osteogenic differentiation of human mesenchymal stem cells (hMSCs) *in vitro* without use of any other osteoinductive factors, e.g., BMPs or dexamethasone [16]. This pro-osteoblastic activity of NS is possibly because of the nontoxic degradation products, e.g., Mg^{2+}, Si (OH) $_4$, and Li^{+} as well as the interactions with cellular components [15, 22–26]. It is very attractive and advantageous for bone tissue engineering if NS has intrinsic osteoinductive activity. However, no study has reported that NS alone can induce ectopic bone regeneration so far. Our most recent study revealed that NS had very limited osteogenic activity on mouse pre-osteoblast cells *in vitro* and failed to induce ectopic bone formation, while NS can significantly improve BMP2-induced ectopic bone regeneration in mice [18]. Therefore, the main contribution of NS to bone formation needs to be further studied.

Other than the potential pro-osteoblastic activity, some groups reported that the mechanical properties of scaffolds with NS showed a marked increase by virtue of the strong polymer-

nanoclay interaction [17, 19]. The improved stiffness may contribute to elevated hMSCs' osteogenic differentiation and bone regeneration since mechanical properties of biomaterials play a vital role in stem cell osteogenic differentiation [27–30]. Unfortunately, the majority of current studies on NS were focused on hydrogel materials [17, 19–21] which are not ideal for investigation of the role of NS in bone repair due to the poor mechanical properties, and the lack of interconnected macro-pores and biomimetic nano/microstructures.

To better understand the role of NS in three-dimensional (3D) polymer scaffolds for bone tissue engineering, we recently developed a novel NS-modified 3D gelatin nanofibrous scaffold (GF/NS) by a thermally induced phase separation technique together with the particle leaching method (TIPS&P) with defined macro-pore structures and collagen-like nanofibers [18]. NS significantly improved Young's modulus of the composite scaffolds, while maintaining similar macro and micro-structure with the neat gelatin scaffolds. Besides the improved mechanical properties, GF/NS scaffolds displayed significantly higher absorbance of proteins compared to the neat GF scaffold [18], which is likely attributed to the strong NS-drug binding ability [31]. These composites scaffolds (GF/NS) not only promoted the osteoblastic differentiation *in vitro* but also significantly improved BMP2-induced ectopic bone formation in mice. In fact, NS has demonstrated strong drug binding and sustained release capacity for many types of molecules [19, 31–33] because of a high specific surface area and charge anisotropy [15, 34, 35]. Therefore, we still don't know the primary mechanism of NS for the improved bone formation although our previous work suggests that NS-enabled drug binding and improved mechanical property of scaffolds are more important than the intrinsic osteoinductivity in the ectopic bone formation mouse model.

The critical knowledge gap mentioned above will significantly impede NS-based biomaterials design and consequent application in bone tissue engineering. To determine the primary role of NS in osteoblastic differentiation *in vitro* and bone formation *in vivo*, we used the mouse calvarial-derived pre-osteoblasts (MC3T3-E1 cells) and a clinically-relevant mouse cranial bone defect model in our current study. The essential roles of NS-enabled drug binding/sustained release and improved mechanical properties in critical low-dose BMP2 (0.5 μg per scaffold)-induced mouse cranial bone regeneration were determined on both 3D GF and NS-incorporated composite scaffolds (GF/NS). Instead of the primarily studied hydrogel systems, our 3D scaffolds with defined macro-pores and bone-matrix mimicking nanofibrous structures provided us an advantageous tool to better study NS's functions in bone regeneration.

2. Materials & Methods

2.1. Materials

Gelatin from bovine skin (225 Bloom, type B), ethanol, 2-(N-morpholino)-ethanesulfonic acid hydrate (MES hydrate), *N*-(3-Dimethylaminopropyl)-*N'*-ethylcarbodiimide hydrochloride (EDC), N-hydroxysuccinimide (NHS), 1, 4-dioxane, cyclohexane, molecular biology grade water, and β-glycerophosphate salt were purchased from Sigma (St. Louis MO, USA). Hexane and Bovine Serum Albumin (BSA) were purchased from Fisher Scientific (New Jersey, USA). Recombinant human BMP2 (rhBMP2) and BMP2 Mini

ABTS ELISA Development Kit were bought from Peprotech (Rocky Hill, NJ, USA). Nanoclay was kindly gifted by Southern Clay Products, Inc. (Louisville, USA).

2.2 Preparation of 3D gelatin nanofibrous (GF) and GF/NS Scaffolds

3D GF scaffolds were prepared according to our previous works [18, 36, 37]. In brief, 40 °C 50% v/v ethanol/water mixed solvent was used to dissolve gelatin type B to make a 10% w/v uniform gelatin solution. The porogen (150 to 300 μm sized paraffin spheres, PS) was prepared in advance for GF scaffolds. Then 10% w/v gelatin solution was poured into PS template and immediately transferred into a −80 °C freezer for overnight phase separation. The frozen samples were then immersed into ethanol and 1, 4-dioxane for 24 h, respectively, followed by −80 °C overnight, and then 48 h lyophilization. The Gelatin-PS composite scaffolds were cut into 5mm width and 1mm height discs by Premier Biopsy Punch (Plymouth Meeting, PA, USA) and soaked in hexane to remove PS. Residual hexane was exchanged by fresh cyclohexane every 2 h for 8 h. Finally, samples were lyophilized for 48 h and kept dry in a desiccator for future experiments.

For the preparation of GF/NS scaffolds, NS (12 mg/mL) was dissolved in 50% v/v ethanol/water mix solution. After that, NS solution was mixed with 13.33% w/v gelatin solution at a ratio of 1:3 (v/v) and poured into paraffin spheres followed by the same procedures utilized for GF scaffolds preparation. The final concentration of NS and gelatin B here was 3mg/mL and 10% (w/v), respectively. MES buffer (0.05 M, pH 5.3) together with EDC and NHS was used for GF and GF/NS scaffolds chemical crosslinking. The crosslinking progress was carried out for 24 h in ice-cold acetone at the ratio of acetone/cross-linking agents (90/10). The crosslinking process was stopped by immersing the scaffolds into glycine solution, and then scaffolds were washed in distilled water 3 times, frozen at −80 °C overnight, and finally lyophilized for 48 h.

2.3. Surface characterization GF and GF/NS scaffolds

Surface microstructure and morphologies of 3D GF and GF/NS scaffolds were characterized by a Hitachi S-4800 Scanning Electron Microscopes. Samples were sputter coated with gold and imaged at an accelerating voltage of 5 kV. The Energy Dispersive X-Ray Spectroscopy (EDS) spectra was recorded with the Hitachi S-4800, with an installed IXRF EDS system for EDS imaging.

2.4. Cell culture and cell viability study

Minimum Essential Medium Alpha (1X) (α-MEM, Gibco, Waltham, MA), supplemented with 10% fetal bovine serum (FBS), 100 mg/mL streptomycin sulfate, and 100 U/mL penicillin was used as the normal Growth Medium. Mouse calvarial-derived pre-osteoblasts (MC3T3-E1, from ATCC) were cultured in Corning® T-75 flasks under a humidified atmosphere with 5% CO_2 at 37 °C. Growth medium was changed twice per week. MC3T3-E1 cells were passaged when they reached around 90% confluence. Passages between 9 and 10 were used for this research. To induce MC3T3-E1 cells osteoblastic differentiation, cells were cultured in an osteoconductive medium (the normal growth medium containing 50 μg/mL L-ascorbic acid and 2.5 mM β-glycerophosphate salt).

Cytotoxicity of NS on MC3T3-E1 cells was quantitatively measured using a CellTiter 96® AQ_{ueous} One Solution Cell Proliferation Assay (MTS) according to the product instructions (Promega, Madison, WI, USA). In short, 1×10^4 MC3T3-E1 cells were seeded into each well. On day 0, 1 and 4, the growth medium was removed, and fresh serum-free medium containing 20% MTS reagent was added into each well and incubated at 37 °C for 2 h in a humidified and dark 5% CO_2 atmosphere. Reacted medium of each sample was then transferred into a 96-well plate. Absorbance of samples was read at 490 nm using a SpectraMax M2e Microplate Reader (Molecular Devices, San Jose, CA, USA).

Cell morphologies of MC3T3-E1 on day 0 and day 4 were visualized by staining with fluorescent Phalloidin-FITC (Life Technologies, OR, USA) and DAPI (Sigma, St. Louis MO, USA) according to the manufacturer's manual. In brief, cells were fixed for 15 min by 3.7% methanol-free formaldehyde and then permeabilized in 0.1% TritonX-100 for another 15 min. After that, cells were stained with fluorescent Phalloidin and DAPI for 40 and 5 min, respectively. Samples were then observed under confocal microscopy (Zeiss LSM 710, Germany).

2.5 Alkaline phosphatase (ALP) activity

1×10^4 MC3T3-E1 cells were seeded into a 24-well plate with growth medium and incubated at 37 °C containing 5% CO_2. After overnight incubation, the growth medium was replaced with an osteoconductive medium. After 7 days cell culture, the ALP activity was quantified and qualified with an EnzoLyte pNPP Alkaline Phosphatase Assay Kit (AnaSpec, San Jose, CA, USA), following the product manual [38, 39]. In brief, samples were rinsed with DPBS and lysed for 5 min at room temperature. Collected lysate was transferred into a centrifuge tube, incubated on ice for 10 min under mild shaking, and centrifuged for 10 min at 2500×g under 4 °C. The supernatant/standard solution (50 uL) was mixed with p-nitrophenyl phosphate (room temperature) and incubated at 37°C for 30 min. ALP activity was then tested at 405 nm and normalized against total protein content, which was measured by a BCA kit (Thermo Scientific™, Waltham, MA, USA) based on the user instructions. In short, 25 uL collected supernatant (same from the former ALP activity experiment)/standard solution was homogeneously mixed with 200 uL of BCA working solution, incubated at 37 °C for 30 min, and measured at 562 nm.

ALP histochemistry was evaluated using an Alkaline Phosphatase Staining Kit (Sigma, St. Louis MO, USA) follow the product instruction. Cells were fixed by Citrate-Acetone-Formaldehyde mixed solution for 30 s and followed by 45 s rinse with distilled water. The fixed cells were then stained by a diazonium salt/Naphthol AS-Bl Alkaline solution for 15 min in dark at room temperature, rinsed for 2 min by distilled water. The ALP staining images were taken via a camera (Canon PSSX420IS, Japan).

2.6 Alizarin red S (ARS) staining and quantification

ARS staining was used to detect the calcium-rich deposits by cells according to our previous protocols [37] with a minor modification. Briefly, after 21 days of cell culture, cells were rinsed with DPBS and fixed in 70% ice-cold ETOH for at least 1h, washed with distilled water and stained by 40 mM ARS solution (Sigma, pH to 4.2 by 1M hydrochloride acid) for

10 min at room temperature under shaking. For the quantification of the ARS staining, 10% w/v cetylpyridinium chloride (CPC) (Sigma St. Louis MO, USA) was prepared and added 1 mL/well and incubated for 30 min to elute the stain. The eluted dye was measured at 550 nm using a microplate reader (Molecular Devices, San Jose, CA, USA).

2.7 Quantitative gene analysis

The osteogenic biomarkers including Runt related transcription factor 2 (*Runx2*), osteocalcin (*OCN*), and bone sialoprotein (*BSP*) were analyzed on day 7 using real-time PCR. Quantitative gene expression analysis was carried out according to the product instructions. Briefly, total cellular RNA was extracted using a miRNeasy Mini Kit (Qiagen, Valencia, CA). The concentration of total RNA was measured using a NanoDrop™ One spectrophotometer (Thermo Scientific, Pittsburgh, PA). Equivalent amount of RNA was processed to generate a complementary strand of DNA (cDNA) using an iScript™ cDNA Synthesis Kit (Bio-Rad Hercules, CA). *Runx2*, *OCN*, and *BSP* were expressed on a CFX Connect™ (Bio-Rad Hercules, CA) utilizing the iQ SYBR® Green Supermix Kit (Bio-Rad Hercules, CA). Gene primers of *Runx2* (qMmuCED0049270) and *OCN* (qMmuCED0041364) were purchased from Bio-Rad (Hercules, CA), while the housekeeping gene glyceraldehyde 3-phosphate dehydrogenase (GAPDH) and *BSP* were synthesized at the University of Iowa (Table S1).

2.8. rhBMP2 release from GF and GF/NS scaffolds

The influences of NS binding ability for *in vitro* BMP2 release were studied on GF+BMP2, GF/NS+BMP2, and GF+BMP2/NS scaffolds. NS was prepared in molecular biology grade water. Prior to the sterilization of GF and GF/NS scaffolds, NS (1 mg/mL final concentrations in scaffolds) was premixed with rhBMP2 (Peprotech, Rocky Hill, NJ, USA, 100 ng per scaffold) overnight to ensure binding of the protein to NS. The BMP2/NS mix solution was blended with collagen I (2.5 mg/mL, Bedford, MA, USA) and a total of 10 μL collagen+BMP2/NS mix solution was loaded onto GF scaffolds. The same amount of collagen+BMP2 mixture without NS was added onto GF and GF/NS scaffolds as controlled groups. Following gelation at 37 °C for 30 minutes, bovine serum albumin in 1X DPBS (release buffer) was added to the scaffolds+BMP2 and placed in a 37 °C shaker. The BMP2 release supernatants were removed and replaced with fresh release buffer at specific time points. After 28 days of release, a human/murine/rat BMP-2 ELISA kit (Peprotech, USA) was used per our previous protocol [37] to detect rhBMP2 release from the scaffolds.

2.9. *In vivo* bone regeneration

Laboratory animals' care and use were followed by the protocols approved by the office of the Institutional Animal Care and Use Committee (IACUC) of the University of Iowa. Inbred C57BL/6NHsd female mice (6 weeks, ENVIGO) were used to create the large size cranial bone defect model (~3 mm in diameter) for *in vivo* bone regeneration study [40, 41]. 1mg/mL NS (final concentration in scaffolds), 0.5 μg BMP2/scaffold or BMP2/NS mix (the same preparation procedure as section 2.8) was homogeneously suspended in 10 μL of collagen I and then loaded into gelatin nanofibrous scaffolds (GF) and NS-blended composite scaffolds (GF/NS). 30 mice were used in this animal study, divided into 6 groups (n = 5) and treated as the groups: GF, GF/NS, GF+BMP2, GF/NS+BMP2, GF+NS, and GF

+BMP2/NS. 6 weeks after surgery, all the mice were euthanized, and the retrieved samples were fixed in 10% neutral formalin for two days and then transferred into 70% cold-ethanol for further analysis.

Radiographic analysis was carried out on the fixed constructs using a Zeiss Xradia 520 Versa (Pleasanton, CA). A microCT (μCT, SkyScan 1272, Bruker) analysis was used to study new bone formation at the defect place. Micro-computed tomography was done utilizing SkyScan software, where specimens were mounted upright and scanned 180 degrees at 0.6-degree intervals, with a resolution of 16 μm. Image reconstruction and volume analysis were done via NRecon software and CTAnalyser software, respectively. Bone volume (BV)/ Tissue volume (TV) was used to calculate new bone formation via CTAnalyser software. 3D volume rendering and 3D imaging of the defect area were completed using the CTvox software. A singular CT threshold was applied to all samples when calculating BV/TV.

Hematoxylin and Eosin (H&E) stain was used for histological analysis. Briefly, the samples were decalcified in 15% EDTA (Fisher Scientific, New Jersey, USA) for 2 days and kept in 70% ethanol. After that, the samples were embedded into paraffin wax, and cross-sections of 5 μm were cut from the middle of scaffolds. These sections were H&E stained and observed under a microscope.

2.10 Statistical analysis

All analyses were performed with Origin version 9.1 software. Data were presented as means ± standard deviation. The means for three or more parallel groups were analyzed by one-way ANOVA. $*p < 0.05; **p < 0.01; ***p < 0.001$ were identified as statistically significant between individual groups.

3. Results

3.1 Cytotoxicity of NS on MC3T3-E1 cells.

The cytotoxicity of the NS on MC3T3-E1 cells was quantitatively measured by MTS assay after culturing for 0, 1, and 4 days. As the data showed, cells exhibited similar viability on day 0 (2 hours after the NS treatment, Fig. 1A). The cell viability was positively correlated with the incubation time. However, after 1 day incubation, significant cytotoxicity of NS on the viable cells was observed when treated at a high concentration (1000 μg/mL) compared to the control group ($P < 0.001$). On day 4, significant cytotoxicity was observed at all the tested concentrations of NS in contrast to the control group, which is consistent with our previous report that NS has mild cytotoxicity on hMSCs after 3 days' culture. Therefore, the low concentration of NS was chosen as 50 μg/mL to minimize the cytotoxicity in the following in vitro studies. Cell morphology of MC3T3-E1 cells was imaged after treating with or without 50 μg/mL of NS for 2 hours (Day 0) and 4 days (Day 4) (Fig. 1B & C). Confocal imaging demonstrated no obvious differences in cell morphology between treatment and control group on day 0. However, after 4 days of incubation, compared to the control group (Fig. 1C1), a significant amount of NS aggregation was noticed (Fig. 1C2), where the white arrow indicated adherence and internalization of NS nanoparticles in MC3T3-E1 cells.

3.2 Effects of NS on BMP2-induced osteogenic differentiation

To study the effects of the NS and BMP2 on MC3T3-E1 cells osteogenic differentiation, we investigated the ALP activity and mineralization degree *in vitro*. After 7 days culture, the single-dose of BMP2 (OC+BMP2 ×1), multiple-dose of BMP2 (OC+BMP2 ×2), and BMP2/NS mix one-time treatment (OC+BMP2/NS mix x1) groups showed significantly higher ALP activity compared to the OC alone group, although the NS single-dose treatment (OC+NS x1) group did not raise the ALP much (Fig. 2A, B).

To further study the effects of NS on MC3T3-E1 cells osteogenic differentiation, we measured the mineralization of cultured cells through Alizarin Red S staining and CPC quantification after 3 weeks of cell culture (Fig.2C, D). Consistent with our ALP activity data, considerably higher mineralization of MC3T3-E1 cells was found on the BMP2 multiple treatment group (OC+BMP2 ×6) and OC+BMP2/NS mix x1 group compared to that from the OC control group, while there was no significant difference between the BMP2 multiple treatment groups (OC+BMP2 ×2 and OC+BMP2 ×6) and BMP2/NS one time treatment group (OC+BMP2/NS mix x1). These results suggest that the NS binding with BMP2 played a crucial role in BMP2-induced osteogenic differentiation.

3.3. Gene expression

After 7 days incubation in OC medium, the quantitative gene expression of osteogenic markers *Runx2*, *OCN*, and *BSP* was evaluated to further demonstrate the effect of the BMP2 and NS to enhance osteogenic differentiation. *Runx2* protein does not show any significant difference between all the samples, but there was an up-regulation trend of all 4 treatment groups, compared with the OC control group (Fig. 3, left). The OC+BMP2 ×1, OC+BMP2 ×2, and OC+BMP2/NS mix x1 groups demonstrated significantly higher *BSP* expression compared to the OC control group, although the OC+NS x1 group did not up-regulate much (Fig. 3, right). Consistent with ALP activity and CPC quantification data (Fig. 2), both OC +BMP2 ×2 and OC+BMP2/NS mix x1 groups demonstrated significantly higher mature osteogenic marker *OCN* expression. Moreover, no significant difference was found between the BMP2 multiple treatment group (OC+BMP2 ×2) and BMP2/NS one time treatment group (OC+BMP2/NS mix x1) (Fig. 3, middle), further indicating the necessity of NS binding with BMP2 for BMP2-induced osteogenic differentiation.

3.4. Characterization of GF and GF/NS scaffolds

SEM images showed neat 3D GF scaffolds have interconnected macroporous structure (10% gelatin, pore size=150 to 300 μm, Fig.4 A) and collagen-like nanofibrous microstructures (Fig.4 B–C). After NS incorporation, the interconnected pore structure (Fig.4 D, containing 3 mg/mL NS in 10% gelatin) and nanofibrous microstructure (Fig.4 E–F) were maintained after freeze-drying, which was similar to the previous reports [18, 37]. The EDS analysis results of the GF and GF/NS scaffolds revealed the presence of higher Na, Si, and Mg (Table 1) in GF/NS scaffolds.

3.5. In-vitro Release Study of BMP2 from scaffolds

The release curves of BMP2 from GF+BMP2, GF/NS+BMP2, and GF+BMP2/NS are displayed in Fig. 5. Compared to GF+BMP2/NS group, a significantly higher initial burst

release was found in both GF+BMP2 and GF/NS+BMP2 groups (Fig. 5A), followed by a continuous release during the duration of the experiment (28 days, Fig. 5B). Interestingly, the overall release profiles of the GF+BMP2 and GF/NS+BMP2 groups were similar, while significantly higher total amounts of BMP2 were noted from GF+BMP2/NS scaffolds than both the GF+BMP2 and GF/NS+BMP2 groups (~26500 pg vs ~17000 pg). These data indicated that direct NS binding with BMP2 could support the long-time continuous/sustained release of BMP2 from the 3D GF scaffolds. Moreover, the NS was able to protect the fragile protein from fast degradation compared to the simple loading of BMP2 alone, since the same amount of BMP2 was incorporated in three groups (100 ng per scaffold).

3.6. BMP2 binding with NS Significantly Promote Endogenous Bone Regeneration

NS has shown varied proposed functions, e.g., osteoinductivity, improving mechanical properties and drug binding abilities based on both others' [15, 18, 24, 31] and our work (Fig. 5). Although our previous work suggests that NS-enabled drug binding and improved mechanical property of scaffolds are more important than the intrinsic osteoinductivity in the ectopic bone formation mouse model, we still don't know the exact mechanism of NS for the improved bone formation. To better understand the role of NS in a 3D gelatin nanofibrous scaffold for bone regeneration, new bone formation on the neat GF and GF/NS scaffolds was studied by using the mouse calvarial defects (with or without rhBMP2, BMP2 alone or NS binding with BMP2).

After 6 weeks of implantation, the GF+BMP2/NS group demonstrated a significantly higher amount of newly formed bone in the defects than other groups. The macro-views of H&E stained slides show the locations of the scaffolds, bone defects, new bone formation and adjacent tissues (upper panel, Fig. 6). The radiographic testing results revealed that no obvious new bone tissues were formed in all of the implanted scaffolds, even those supplemented with a low dose of BMP2 (0.5μg per scaffold, lower panel, Fig. 6), except the GF+BMP2/NS group.

Higher magnification (10×) histological images confirmed that very few bone-like tissues (pink color) were observed inside the transplanted scaffolds (purple color) in GF, GF/NS, GF+BMP2(0.5μg), GF/NS+BMP2(0.5μg), GF+NS(1mg/mL) groups, while significantly higher new bone formation was detected in GF+BMP2/NS groups (4/5, Fig. 7F), which is consistent with our radiographic examination observation (lower panel, Fig. 6).

Consistently, as seen by μCT results, no significant bone formation was observed in the GF, GF/NS, and GF+BMP2 group. However, NS binding with BMP2 group (GF+BMP2/NS) induced newly formed bone tissue completely covering the defects (Fig. 7h, right panel). Quantitatively, bone defects implanted with GF+BMP2/NS had ~14.5% increase in new bone formation, whereas the GF group with a much lower BV/TV only had a ~0.64 % increase, the GF/NS group had a ~1.6% increase, and the GF+BMP2 group revealed a ~ 1.48% increase (Fig. 7I).

Hence, our *in vivo* results indicated that supplement of an extremely low dose of rhBMP2 (0.5 μg/scaffold) was not able to induce mouse cranial bone formation even with the incorporation of NS in scaffolds, although we previously reported that the GF/NS scaffolds

significantly improved BMP2-induced ectopic bone formation in mice (1.5 g BMP2 per scaffolds)[18]. NS-enabled drug binding/sustained release plays an essential role in the promotion of endogenous bone formation in the mice cranial bone defect model.

4. Discussion

One advantage for NS's application in regenerative medicine and drug delivery is its high biocompatibility and low cytotoxicity [18]. However, our *in vitro* data indicated NS had significant cytotoxicity on MC3T3-E1 after 4 days of culture even at the lowest tested dosage (50 μg/mL). This suggested mouse preosteoblasts (MC3T3-E1) were more sensitive to NS treatment compared to hMSCs since NS had no significant detrimental effects on hMSCs at 100 μg/mL based on previous reports [18, 24]. Cell morphology images also confirmed that NS adheres to the cell surface and is internalized, which might restrict cellular functionality in long term cell culture. Therefore, we chose the low dose (50 μg/mL) of NS for the *in vitro* experiments to minimize the cytotoxicity of NS on cell differentiation. Our data indicate 50 μg/mL of NS was capable of improving BMP2-induced osteoblastic differentiation. However, much higher dose of NS had to be used to achieve the sustained release of proteins/small molecules and reduce the burst release. Based on our preliminary tests, 1000 μg/mL was the minimal dose required for sustained release of BMP2, which therefore was used for *in vivo* studies. Interestingly, 1000 μg/mL of NS didn't cause inflammatory/toxic side effects as it did *in vitro* cell culture. Therefore, our data confirmed that NS had good biocompatibility which was possibly because of the interaction with the plenty of extracellular matrix/proteins *in vivo*. This data suggested the importance of *in vivo* studies for understanding the mechanism of NS in bone regeneration.

NS is especially attractive for bone tissue engineering since it has demonstrated potential inherent osteoinductivity as some studies suggested [15, 16, 42]. However, our recent findings indicated that NS failed to induce ectopic bone formation when it was blended into 3D GF scaffolds [18]. It was known that the composite scaffolds with higher mechanical properties were capable of improving BMP2-induced ectopic bone formation [18] as ectopic bone formation ability is the gold standard to evaluate if the materials have osteoinductive ability [43, 44]. We strongly believe that NS contributes to the improved bone regeneration primarily through other ways than its inherent osteoinductivity in mice. To further understand the mechanism of NS in bone regeneration, we used the mouse calvarial-derived preosteoblast MC3T3-E1 instead of hMSCs. Consistent to our previous report, NS alone was not capable of significantly improving osteoblastic differentiation of MC3T3-E1. Importantly, ALP activity, matrix mineralization, and gene expression results revealed one dose of NS directly mixed with BMP2 could significantly improve osteoblastic differentiation. As the control, multiple doses of BMP2 were required to achieve sufficient differentiation without mixing with NS because BMP2 like other proteins degraded and lost bioactivity very quickly in aqueous solution [38]. Therefore, super high dosage of BMP2 needed in the applications subsequently could cause severe side-effects which represents a significant clinical challenge [45, 46]. This interesting data suggested that direct interaction with NS was important to maintain/improve the bioactivity of BMP2 for osteoblastic differentiation. Our release data further confirmed that NS not only provided sustained release but also protection of BMP2 because significantly more bioactive proteins were

detected from NS binding group compared to other groups without direct binding with NS. Consistent to our previous report, GF/NS composite scaffolds also slightly reduced the burst release of BMP2 at the early stage possibly because of NS-endowed high affinity [18], while much less effective than the direct binding group.

Compared to ectopic bone formation model, orthotopic cranial bone defect model is more clinically relevant for us to explore the role of NS in bone tissue regeneration. Although our previous study [18] indicated that NS didn't show the osteoinductivity as it did to hMSCs *in vitro* [15, 16, 24, 42], one possible reason was that NSs were blended with gelatin and embedded in the cross-linked scaffolds which could prevent the direct interactions between the nanoclays with surrounding cells as they did in the solution *in vitro*. The direct interaction with stem cells was one of the potential mechanism that NS could promote hMSCs osteogenic differentiation [15]. Thus, we fabricated both NS blended GF/NS composite scaffolds and GF neat scaffolds loaded with NS solution (GF+NS) to study if NS could induce bone formation in our cranial bone defect model. Notably, neither of these two groups could induce significant new bone formation without exogenous BMP2 addition. Consistent with the release profiles *in vitro*, our *in vivo* data also showed a trend of more new bone formation in the GF/NS+BMP2 group than the GF+BMP2 group, although not significantly. This difference is possibly because we used a much lower dose of BMP2 (0.5 μg per scaffold) in the current cranial bone defects rather than the ectopic bone regeneration we previously reported (1.5 μg BMP2 per scaffold). Importantly, the highest new bone formation in GF+BMP2/NS group highlighted that NS direct binding with BMP2 was much more important and essential for NS improved bone regeneration compared to its other contributions, including the improved mechanical properties and degraded chemicals from the composite scaffolds. Thus, our data strongly demonstrated that NS-mediated drug binding/protection and sustained release played the primary role in nanoclay-improved bone regeneration.

A biocompatible and facile drug delivery system is key for the success of the biomaterial in regenerative medicine, especially bone tissue engineering. Compared to other non-degradable nanoparticles or complicated polymeric micro/nanoparticles, NS is a fascinating 2D nanomaterial for bone regeneration. Some intriguing features include: (1) biocompatibility as many studies indicated [15, 16, 24, 42]; (2) easy processability with polymer scaffolds; (3) biodegradable, especially its' pro-osteoblastic degradation mineral ions which is advantageous for osteoblastic differentiation and bone repair while a lot of nanoparticles, e.g., mesoporous silica nanoparticles (MSNs) and graphene oxide have limited degradability with much higher cytotoxicity and safety concern [16, 47]; (4) easy and mild condition for drug loading, as it can be used to load and prolong the half-life of bioactive molecules; (5) versatility of drug types for delivery, namely drugs/proteins regardless of their charges, as hydrophobic and hydrophilic compounds can bind with NS due to its large surface area and the existence of anisotropic charges [17, 19, 31, 48, 49]; (6) the drug release rate is tunable by adjusting the ratio or content of NS, and the drug release extent was proved to be negatively correlated with the NS concentration [31]. The biomaterials-based cell-free strategy is the ultimate goal for tissue engineering since it is more straightforward and less complicated and more translational-able than cell-based therapy [50]. Combination of the potent drug release/pro-osteoblastic ability of NS and

biomimetic 3D scaffold make the cell-free bone regenerative strategies more realistic which promote bone regeneration by activating and harnessing the endogenous reparative cells and signals.

Overall, our work indicated that the direct binding of NS with BMP2 and enabled subsequently sustained release is the primary reason among other contributions for the nanoclay-promoted bone regeneration by using a clinically relevant mouse cranial bone defect model and biomimetic 3D scaffolds.

5. Conclusions

In this study, we investigated the potential mechanisms underlying the roles of NS to osteoblastic differentiation and new bone formation. Our *in vitro* results confirmed that NS was biocompatible and NS direct binding with BMP2 not only provided sustained release but also protected the bioactivity of BMP2. Our data from the cranial bone defects models further indicated, compared to NS-improved mechanical properties and intrinsic osteoinductivity, NS direct binding with BMP2 enabled sustained and prolonged drug release is much more important for NS enhanced bone regeneration in mice, especially when supplemented with critically low-dose of BMP2 (0.5 μg per scaffold). Most importantly, we give a better knowledge of the roles of NS in new bone formation and provide a safe, low-cost, and efficient delivery system for bone regeneration.

Supplementary Material

Refer to Web version on PubMed Central for supplementary material.

Acknowledgments

This work was supported by the startup funds from the Department of Oral and Maxillofacial Surgery at the University of Iowa, the National Institute of Dental & Craniofacial Research of the National Institutes of Health under Award Numbers R03DE027491, R01DE029159, and T90DE023520. The content is solely the responsibility of the authors and does not necessarily represent the official views of the National Institutes of Health. The authors also would like to thank Dr. Brad A. Amendt and the members of his lab for their support in microscope usage.

Reference

[1]. Petite H, Viateau V, Bensaïd W, Meunier A, de Pollak C, Bourguignon M, Oudina K, Sedel L and Guillemin G. Tissue-engineered bone regeneration[J]. Nature Biotechnology: 2000 18(9): 959–963. 10.1038/79449

[2]. Cancedda R, Giannoni P and Mastrogiacomo M. A tissue engineering approach to bone repair in large animal models and in clinical practice[J]. Biomaterials: 2007 28(29): 4240–4250. 10.1016/j.biomaterials.2007.06.023 [PubMed: 17644173]

[3]. Ng MH, Duski S, Tan KK, Yusof MR, Low KC, Rose IM, Mohamed Z, Bin Saim A and Idrus RBH. Repair of segmental load-bearing bone defect by autologous mesenchymal stem cells and plasma-derived fibrin impregnated ceramic block results in early recovery of limb function[J]. BioMed Research International: 2014 2014: 345910 10.1155/2014/345910 [PubMed: 25165699]

[4]. Greenwald AS, Boden SD, Goldberg VM, Khan Y, Laurencin CT and Rosier RN. Bone-Graft Substitutes: Facts, Fictions, and Applications[J]. J Bone Joint Surg Am: 2001 83(2): 98–103. 10.2106/00004623-200100022-00007 [PubMed: 11712842]

[5]. Amini AR, Laurencin CT and Nukavarapu SP. Bone tissue engineering: recent advances and challenges[J]. Critical reviews in biomedical engineering: 2012 40(5): 363–408. https://pubmed.ncbi.nlm.nih.gov/23339648 [PubMed: 23339648]

[6]. Lad SP, Bagley JH, Karikari IO, Babu R, Ugiliweneza B, Kong M, Isaacs RE, Bagley CA, Gottfried ON, Patil CG and Boakye M. Cancer after spinal fusion: the role of bone morphogenetic protein[J]. Neurosurgery: 2013 73(3): 440–449. 10.1227/NEU.0000000000000018 [PubMed: 23756740]

[7]. Rahmany MB and Van Dyke M. Biomimetic approaches to modulate cellular adhesion in biomaterials: A review[J]. Acta Biomaterialia: 2013 9(3): 5431–5437. 10.1016/j.actbio.2012.11.019 [PubMed: 23178862]

[8]. Gothard D, Smith EL, Kanczler JM, Rashidi H, Qutachi O, Henstock J, Rotherham M, El Haj A, Shakesheff KM and Oreffo RO. Tissue engineered bone using select growth factors: A comprehensive review of animal studies and clinical translation studies in man[J]. Eur Cell Mater: 2014 28: 166–207. 10.22203/ecm.v028a13

[9]. Madhurakkat Perikamana SK, Lee J, Ahmad T, Jeong Y, Kim D-G, Kim K and Shin H. Effects of Immobilized BMP-2 and Nanofiber Morphology on In Vitro Osteogenic Differentiation of hMSCs and In Vivo Collagen Assembly of Regenerated Bone[J]. ACS Applied Materials & Interfaces: 2015 7(16): 8798–8808. 10.1021/acsami.5b01340 [PubMed: 25823598]

[10]. Yao Q, Sandhurst ES, Liu Y and Sun H. BBP-Functionalized Biomimetic Nanofibrous Scaffold Can Capture BMP2 and Promote Osteogenic Differentiation[J]. Journal of materials chemistry. B: 2017 5(26): 5196–5205. 10.1039/C7TB00744B [PubMed: 29250330]

[11]. Zhou Q, Ren X, Bischoff D, Weisgerber DW, Yamaguchi DT, Miller TA, Harley BAC and Lee JC. Nonmineralized and Mineralized Collagen Scaffolds Induce Differential Osteogenic Signaling Pathways in Human Mesenchymal Stem Cells[J]. Advanced healthcare materials: 2017 6(23): 1700641 10.1002/adhm.201700641

[12]. Hou Y, Xie W, Achazi K, Cuellar-Camacho JL, Melzig MF, Chen W and Haag R. Injectable degradable PVA microgels prepared by microfluidic technology for controlled osteogenic differentiation of mesenchymal stem cells[J]. Acta Biomaterialia: 2018 77: 28–37. 10.1016/j.actbio.2018.07.003 [PubMed: 29981495]

[13]. Kim S, Cui ZK, Kim PJ, Jung LY and Lee M. Design of hydrogels to stabilize and enhance bone morphogenetic protein activity by heparin mimetics[J]. Acta Biomater: 2018 72: 45–54. 10.1016/j.actbio.2018.03.034 [PubMed: 29597024]

[14]. Ao Q, Wang S, He Q, Ten H, Oyama K, Ito A, He J, Javed R, Wang A and Matsuno A. Fibrin Glue/Fibronectin/Heparin-Based Delivery System of BMP2 Induces Osteogenesis in MC3T3-E1 Cells and Bone Formation in Rat Calvarial Critical-Sized Defects[J]. ACS Applied Materials & Interfaces: 2020 12(11): 13400–13410. 10.1021/acsami.0c01371 [PubMed: 32091872]

[15]. Xavier JR, Thakur T, Desai P, Jaiswal MK, Sears N, Cosgriff-Hernandez E, Kaunas R and Gaharwar AK. Bioactive Nanoengineered Hydrogels for Bone Tissue Engineering: A Growth-Factor-Free Approach[J]. ACS Nano: 2015 9(3): 3109–3118. 10.1021/nn507488s [PubMed: 25674809]

[16]. Carrow JK, Cross LM, Reese RW, Jaiswal MK, Gregory CA, Kaunas R, Singh I and Gaharwar AK. Widespread changes in transcriptome profile of human mesenchymal stem cells induced by two-dimensional nanosilicates[J]. Proceedings of the National Academy of Sciences: 2018 115(17): E3905–E3913. http://10.1073/pnas.1716164115

[17]. Kim Y-H, Yang X, Shi L, Lanham SA, Hilborn J, Oreffo ROC, Ossipov D and Dawson JI. Bisphosphonate nanoclay edge-site interactions facilitate hydrogel self-assembly and sustained growth factor localization[J]. Nature Communications: 2020 11(1): 1365 10.1038/s41467-020-15152-9

[18]. Yao Q, Fuglsby KE, Zheng X and Sun H. Nanoclay-functionalized 3D nanofibrous scaffolds promote bone regeneration[J]. Journal of Materials Chemistry B: 2020 3842–3851. 10.1039/C9TB02814E [PubMed: 32219244]

[19]. Basu S, Pacelli S, Feng Y, Lu Q, Wang J and Paul A. Harnessing the Noncovalent Interactions of DNA Backbone with 2D Silicate Nanodisks To Fabricate Injectable Therapeutic Hydrogels[J]. ACS Nano: 2018 12(10): 9866–9880. 10.1021/acsnano.8b02434 [PubMed: 30189128]

[20]. Gibbs DM, Black CR, Hulsart-Billstrom G, Shi P, Scarpa E, Oreffo RO and Dawson JI. Bone induction at physiological doses of BMP through localization by clay nanoparticle gels[J]. Biomaterials: 2016 99: 16–23. 10.1016/j.biomaterials.2016.05.010 [PubMed: 27209259]

[21]. Zhang Y, Chen M, Dai Z, Cao H, Li J and Zhang W. Sustained protein therapeutics enabled by self-healing nanocomposite hydrogels for non-invasive bone regeneration[J]. Biomaterials science: 2020 8(2): 682–693. 10.1039/c9bm01455a [PubMed: 31776523]

[22]. Clement-Lacroix P, Ai M, Morvan F, Roman-Roman S, Vayssiere B, Belleville C, Estrera K, Warman ML, Baron R and Rawadi G. Lrp5-independent activation of Wnt signaling by lithium chloride increases bone formation and bone mass in mice[J]. Proc Natl Acad Sci U S A: 2005 102(48): 17406–17411. 10.1073/Fpnas.0505259102 [PubMed: 16293698]

[23]. Han P, Wu C and Xiao Y. The effect of silicate ions on proliferation, osteogenic differentiation and cell signalling pathways (WNT and SHH) of bone marrow stromal cells[J]. Biomaterials Science: 2013 1(4): 379–392. 10.1039/C2BM00108J [PubMed: 32481903]

[24]. Gaharwar AK, Mihaila SM, Swami A, Patel A, Sant S, Reis RL, Marques AP, Gomes ME and Khademhosseini A. Bioactive Silicate Nanoplatelets for Osteogenic Differentiation of Human Mesenchymal Stem Cells[J]. Advanced Materials: 2013 25(24): 3329–3336. 10.1002/adma.201300584 [PubMed: 23670944]

[25]. Yoshizawa S, Brown A, Barchowsky A and Sfeir C. Magnesium ion stimulation of bone marrow stromal cells enhances osteogenic activity, simulating the effect of magnesium alloy degradation[J]. Acta Biomaterialia: 2014 10(6): 2834–2842. 10.1016/j.actbio.2014.02.002 [PubMed: 24512978]

[26]. Thompson DW and Butterworth JT. The nature of laponite and its aqueous dispersions[J]. Journal of Colloid and Interface Science: 1992 151: 236–243. 10.1016/0021-9797(92)90254-J

[27]. Sun H, Zhu F, Hu Q and Krebsbach PH. Controlling stem cell-mediated bone regeneration through tailored mechanical properties of collagen scaffolds[J]. Biomaterials: 2014 35(4): 1176–1184. 10.1016/j.biomaterials.2013.10.054 [PubMed: 24211076]

[28]. Razafiarison T, Holenstein CN, Stauber T, Jovic M, Vertudes E, Loparic M, Kawecki M, Bernard L, Silvan U and Snedeker JG. Biomaterial surface energy-driven ligand assembly strongly regulates stem cell mechanosensitivity and fate on very soft substrates[J]. Proceedings of the National Academy of Sciences: 2018 115(18): 4631–4636. 10.1073/pnas.1704543115

[29]. Engler AJ, Sen S, Sweeney HL and Discher DE. Matrix elasticity directs stem cell lineage specification[J]. Cell: 2006 126(4): 677–689. 10.1016/j.cell.2006.06.044 [PubMed: 16923388]

[30]. Chaudhuri O, Gu L, Klumpers D, Darnell M, Bencherif SA, Weaver JC, Huebsch N, Lee H-P, Lippens E, Duda GN and Mooney DJ. Hydrogels with tunable stress relaxation regulate stem cell fate and activity[J]. Nature materials: 2016 15(3): 326–334. 10.1038/nmat4489 [PubMed: 26618884]

[31]. Koshy ST, Zhang DKY, Grolman JM, Stafford AG and Mooney DJ. Injectable nanocomposite cryogels for versatile protein drug delivery[J]. Acta Biomaterialia: 2018 65: 36–43. 10.1016/j.actbio.2017.11.024 [PubMed: 29128539]

[32]. Aguzzi C, Cerezo P, Viseras C and Caramella C. Use of clays as drug delivery systems: Possibilities and limitations[J]. Applied Clay Science: 2007 36(1): 22–36. 10.1016/j.clay.2006.06.015

[33]. García-Vázquez R, Rebitski EP, Viejo L, de los Ríos C, Darder M and García-Frutos EM. Clay-based hybrids for controlled release of 7-azaindole derivatives as neuroprotective drugs in the treatment of Alzheimer's disease[J]. Applied Clay Science: 2020 189: 105541 10.1016/j.clay.2020.105541

[34]. Delhorme M, Jönsson B and Labbez C. Monte Carlo simulations of a clay inspired model suspension: the role of rim charge[J]. Soft Matter: 2012 8(37): 9691–9704. 10.1039/C2SM25731A

[35]. Angelini R, Zaccarelli E, de Melo Marques FA, Sztucki M, Fluerasu A, Ruocco G and Ruzicka B. Glass–glass transition during aging of a colloidal clay[J]. Nature Communications: 2014 5(1): 4049 10.1038/ncomms5049

[36]. Yao Q, Liu Y, Tao J, Baumgarten KM and Sun H. Hypoxia-Mimicking Nanofibrous Scaffolds Promote Endogenous Bone Regeneration[J]. ACS Appl Mater Interfaces: 2016 8(47): 32450–32459. 10.1021/acsami.6b10538 [PubMed: 27809470]

[37]. Yao Q, Liu Y, Selvaratnam B, Koodali RT and Sun H. Mesoporous silicate nanoparticles/3D nanofibrous scaffold-mediated dual-drug delivery for bone tissue engineering[J]. Journal of controlled release : official journal of the Controlled Release Society: 2018 279: 69–78. 10.1016/j.jconrel.2018.04.011

[38]. Miszuk JM, Xu T, Yao Q, Fang F, Childs JD, Hong Z, Tao J, Fong H and Sun H. Functionalization of PCL-3D electrospun nanofibrous scaffolds for improved BMP2-induced bone formation[J]. Applied Materials Today: 2018 10: 194–202. 10.1016/j.apmt.2017.12.004 [PubMed: 29577064]

[39]. Liu Y, Hu J and Sun H. Mineralized nanofibrous scaffold promotes phenamil-induced osteoblastic differentiation while mitigating adipogenic differentiation[J]. J Tissue Eng Regen Med: 2020 14(3): 464–474. 10.1002/term.3007 [PubMed: 31840422]

[40]. Yao Q, Cosme JG, Xu T, Miszuk JM, Picciani PH, Fong H and Sun H. Three dimensional electrospun PCL/PLA blend nanofibrous scaffolds with significantly improved stem cells osteogenic differentiation and cranial bone formation[J]. Biomaterials: 2017 115: 115–127. 10.1016/j.biomaterials.2016.11.018

[41]. Sun H, Jung Y, Shiozawa Y, Taichman RS and Krebsbach PH. Erythropoietin modulates the structure of bone morphogenetic protein 2-engineered cranial bone[J]. Tissue engineering. Part A: 2012 18(19–20): 2095–2105. 10.1089/ten.TEA.2011.0742

[42]. Jaiswal MK, Xavier JR, Carrow JK, Desai P, Alge D and Gaharwar AK. Mechanically Stiff Nanocomposite Hydrogels at Ultralow Nanoparticle Content[J]. ACS Nano: 2016 10(1): 246–256. 10.1021/acsnano.5b03918 [PubMed: 26670176]

[43]. Shuang Y, Yizhen L, Zhang Y, Fujioka-Kobayashi M, Sculean A and Miron RJ. In vitro characterization of an osteoinductive biphasic calcium phosphate in combination with recombinant BMP2[J]. BMC oral health: 2016 17(1): 35–45. 10.1186/s12903-016-0263-3 [PubMed: 27485617]

[44]. Ana Costa-Pinto Tírcia C. Santos, Neves Nuno M. and Reis RL. Testing Natural Biomaterials in Animal Models[M]. First Edition: John Wiley & Sons 2016: 571 10.1002/9781119126218.ch30

[45]. James AW, LaChaud G, Shen J, Asatrian G, Nguyen V, Zhang X, Ting K and Soo C. A Review of the Clinical Side Effects of Bone Morphogenetic Protein-2[J]. Tissue engineering. Part B, Reviews: 2016 22(4): 284–297. 10.1089/ten.teb.2015.0357 [PubMed: 26857241]

[46]. Lin H, Tang Y, Lozito TP, Oyster N, Wang B and Tuan RS. Efficient in vivo bone formation by BMP-2 engineered human mesenchymal stem cells encapsulated in a projection stereolithographically fabricated hydrogel scaffold[J]. Stem Cell Research & Therapy: 2019 10(1): 254 10.1186/s13287-019-1350-6 [PubMed: 31412905]

[47]. Chen L, Liu J, Zhang Y, Zhang G, Kang Y, Chen A, Feng X and Shao L. The toxicity of silica nanoparticles to the immune system[J]. Nanomedicine: 2018 13(15): 1939–1962. 10.2217/nnm-2018-0076 [PubMed: 30152253]

[48]. Cross LM, Carrow JK, Ding X, Singh KA and Gaharwar AK. Sustained and Prolonged Delivery of Protein Therapeutics from Two-Dimensional Nanosilicates[J]. ACS Applied Materials & Interfaces: 2019 11(7): 6741–6750. 10.1021/acsami.8b17733 [PubMed: 30676016]

[49]. Li K, Wang S, Wen S, Tang Y, Li J, Shi X and Zhao Q. Enhanced In Vivo Antitumor Efficacy of Doxorubicin Encapsulated within Laponite Nanodisks[J]. ACS Applied Materials & Interfaces: 2014 6(15): 12328–12334. 10.1021/am502094a [PubMed: 25000274]

[50]. Sheehy EJ, Kelly DJ and O'Brien FJ. Biomaterial-based endochondral bone regeneration: a shift from traditional tissue engineering paradigms to developmentally inspired strategies[J]. Materials Today Bio: 2019 3: 100009 10.1016/j.mtbio.2019.100009

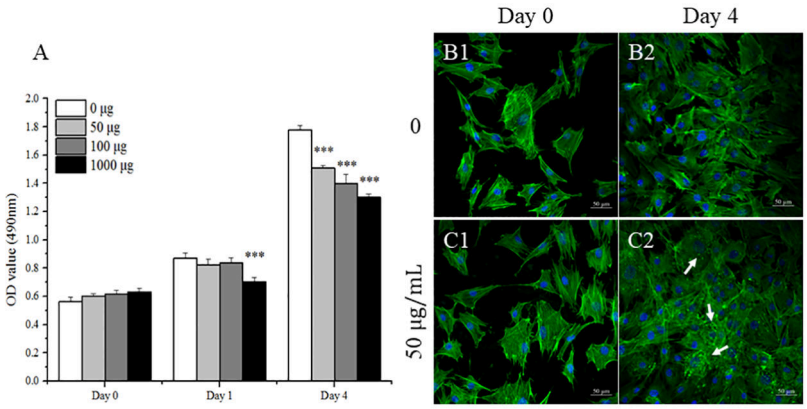

Fig. 1.

Cell viability and morphology of MC3T3-E1 cells after treatment by NS. Cell viability (A) was evaluated after the cells were cultured in growth medium containing with different concentrations of NS for 0, 1, and 4 days (n = 3). Confocal images were taken of MC3T3-E1 cells after treating with (50 μg/mL) and without NS for 2 hours (B1, C1) and 4 days (B2, C2), respectively. Cytoskeletons were shown in green (Fluorescein Phalloidin), while the cell nuclei were blue (DAPI). Scale bar = 50 μm. Arrows indicate aggregations of NS to the cell surface. Results are expressed as mean ± standard deviation (SD) (***p < 0.001 vs.* growth medium control).

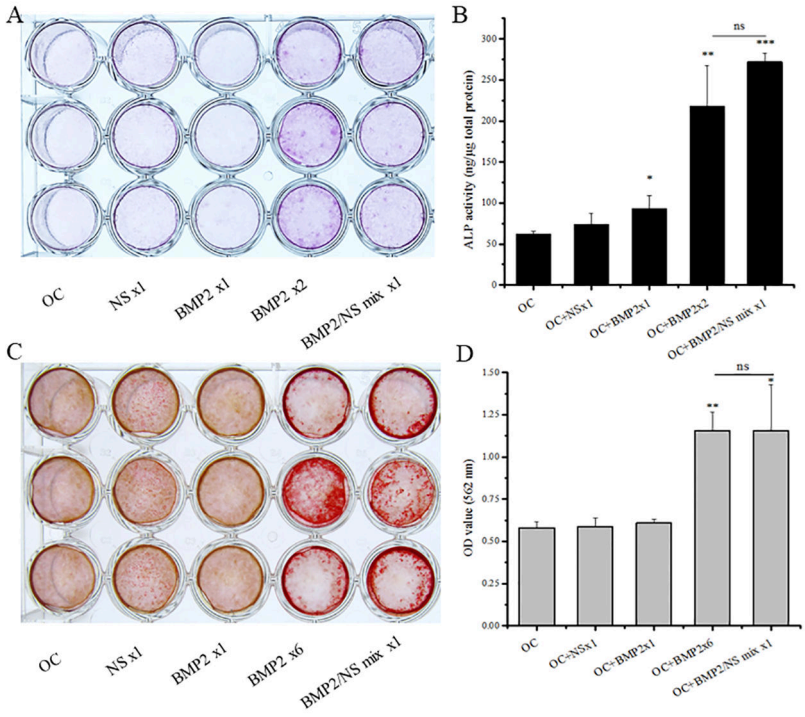

Fig. 2.

Effects of NS on MC3T3-E1 cells osteogenic differentiation. (A) ALP staining, (B) ALP quantification, (C) Alizarin Red S staining and (D) CPC quantification of MC3T3-E1 cells after treatment with different inductive factors in osteoconductive (OC) medium. Data are expressed as mean ±SD, n = 3. (*$P < 0.05$, **$P < 0.01$, ***$P < 0.001$ *vs*. OC control)

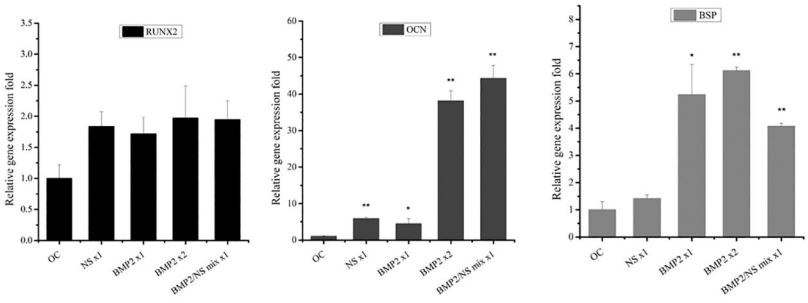

Fig.3.

Osteogenic marker gene expressions (*Runx2*, *OCN* and *BSP*) were quantified by real-time PCR assay after 7 days' culture. Results are presented as mean±SD (n = 3, *$p < 0.05$; **$p < 0.01$ *vs*. OC control)

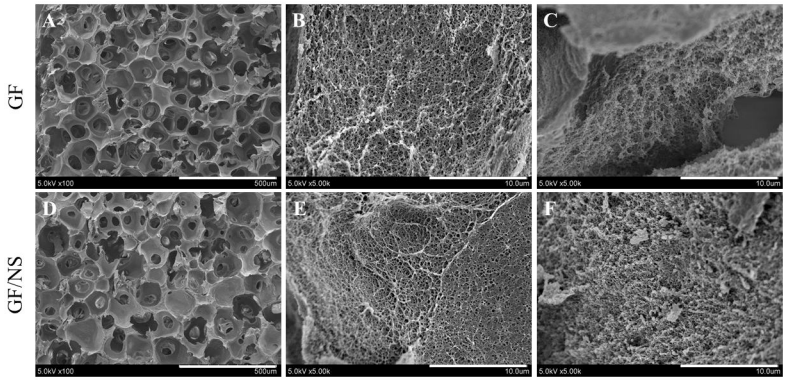

Fig.4.

Characterization of nanofibrous scaffolds. (A-F) SEM images of GF and GF/NS scaffolds at low (scale bars=500 μm, left panel) and high (scale bars=10 μm, middle and right panel) magnifications.

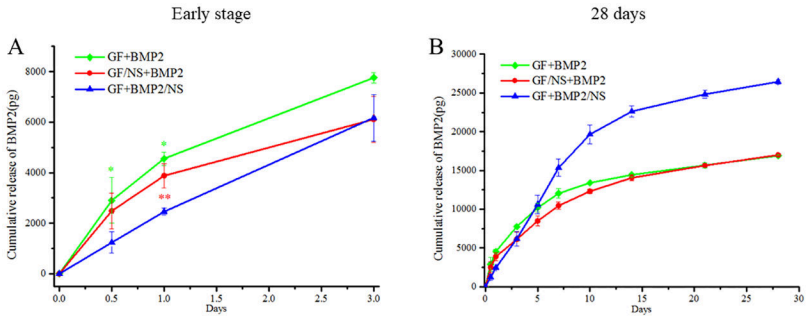

Fig.5.

In vitro release curves of BMP2 from scaffolds. (A) Release profile of early-stage (3 days) (B) long term release properties (28 days). All of the results were represented as means ± SD, n = 3. (*** p < 0.01, * p < 0.05* vs. GF+BMP2/NS)

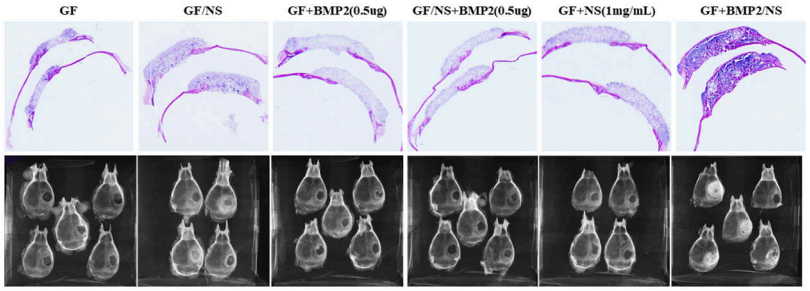

Fig.6.

Digital photos and radiographic testing of the histology samples. GF, GF/NS, GF +BMP2(0.5μg), GF/NS+BMP2(0.5μg), GF+NS(1mg/mL), and GF+BMP2/NS after 6 weeks of implantation (n=4~5).

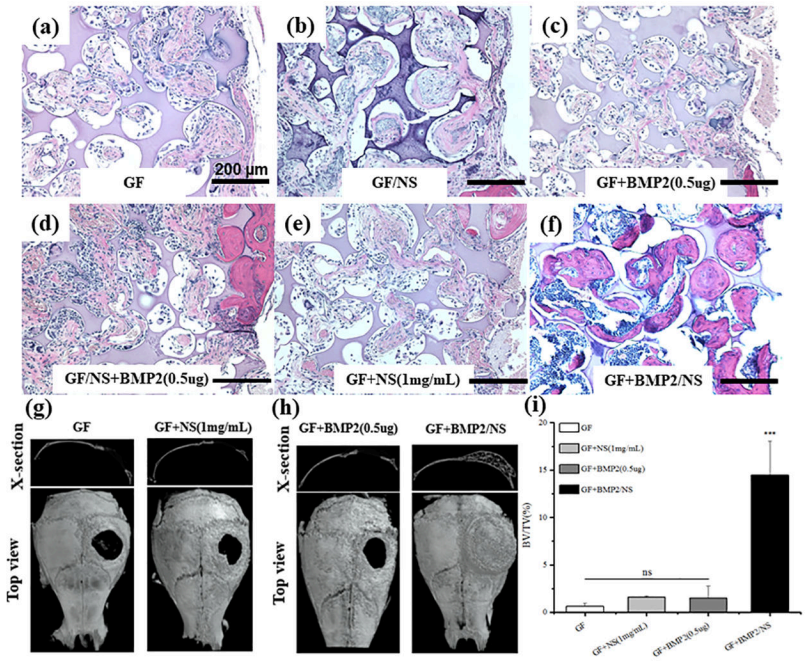

Fig.7.

H&E staining and μCT analysis of the restored calvaries after 6 weeks post-implantation *in vivo*. (A-F) H&E stained tissue sections acquired from the mouse cranial defects (Scale bars=200μm). (G-H) μCT top view and cross-section image of cranial defects. (I) Quantification measurement of BV/TV *in vivo* after implanting different scaffolds. All of the results were expressed as means ± SD (n=4~5, ****P < 0.001 vs.* GF control).

Table.1.

EDS analysis results

Samples	Content of Elements by Weight (%)					
	C	O	Na	Mg	Si	Total
GF	49.15	50.62	0	0	0.23	100
GF/NS	54.52	42.88	0.17	0.94	1.69	100